Characteristics of Tropical Convection over the Ocean near Kwajalein

JASMINE CETRONE AND ROBERT A. HOUZE JR.

Department of Atmospheric Sciences, University of Washington, Seattle, Washington

(Manuscript received 2 February 2005, in final form 30 June 2005)

ABSTRACT

Radar observations have been analyzed to determine characteristics of convection over the oceanic region around Kwajalein in the tropical western Pacific. Generally, the echo areas, heights, and durations exhibited lognormal distributions. Heights were greater under conditions of higher midtropospheric humidity and correlated with echo area, with a wide spread of values. Mergers and splits often truncated echo lifetimes.

The most surprising result was the distribution of orientation angles of echo lines, which statistically verify the shear-parallel and shear-normal modes of convective line organization seen elsewhere over tropical oceans. The two modes typically coexisted within the area of radar coverage, indicating a potential difficulty in predicting line orientation in terms of large-scale variables.

The largest members of the echo population were mesoscale convective systems (MCSs), which had large stratiform components. They occurred in environments of increased humidity and higher midlevel buoyancy associated with westward-propagating synoptic-scale disturbances. MCSs moved with the easterlies in low to midlevels and exhibited the jump updraft, overturning updraft, and subsiding midlevel inflow characteristic of tropical oceanic MCSs.

The Kwajalein Experiment (KWAJEX) radar echo population resembles that of the eastern tropical Atlantic in terms of the shapes of the distributions of area, height, and lifetime, the prevalence of echo mergers and splits, and the tendency to form shear-parallel and shear-normal lines. These characteristics appear to be endemic to oceanic convective populations. Large-scale conditions appear to modulate these basic population characteristics rather than qualitatively alter them.

1. Introduction

Over tropical oceans, convective clouds occur in ensembles that include a broad range of phenomena, from shallow isolated cells to large mesoscale convective systems (MCSs) with both stratiform components and convective cells of various heights (Houze et al. 1980). The convective elements assume different sizes, shapes, orientations, motions, and life cycle behavior. Often one type or another of these clouds is investigated singularly. However, the precipitating clouds of this wide range of sizes and characteristics work in concert to redistribute the mass, heat, moisture, and momentum of the large-scale tropical circulation (Houze 1982, 1989, 1997).

The ensemble properties of convective clouds over the tropical oceans are most readily characterized by measuring the properties of their radar echoes, and several previous studies have attempted to do so. Since even very small convective clouds (tops as low as 1–2 km) precipitate over tropical oceans (Saunders 1965; Rangno and Hobbs 2005), the echo population provides a good indication of the overall convective ensemble properties. Iwanchuk (1973) and López (1976, hereafter referred to as L76) provided information on radar echo sizes, shapes, duration, and motion from the western tropical Atlantic Ocean. Houze and Cheng (1977, hereafter referred to as HC77) and Cheng and Houze (1979) examined similar characteristics for the echo population over the eastern tropical Atlantic using ship radar data collected in the Global Atmospheric Research Program (GARP) Atlantic Tropical Experiment (GATE).

Schumacher and Houze (2003a,b) have shown that the cloud population in the Tropics is not globally uniform. Both the stratiform rain fraction and the shallow, isolated rain fraction vary geographically. However,

Corresponding author address: Jasmine Cetrone, Dept. of Atmospheric Sciences, University of Washington, Box 351640, Seattle, WA 98195-1640.
E-mail: jasmine@atmos.washington.edu

satellite radar data only provide occasional snapshots, are relatively insensitive, and have low spatial resolution. Therefore, they cannot indicate many aspects of radar echo structure, formation, growth, and movement. The satellite radar findings motivate study of other metrics of cloud populations that might vary significantly across the Tropics. Knowing how the precipitating cloud population varies can provide insight into how and where the larger-scale atmospheric circulation is influenced by the convection.

Ground-based radars have the ability to observe the population of a given region continuously over time. They also can have higher resolution and sensitivity than a space-borne radar. These capabilities allow a wider range of convective population properties to be determined than is possible from the satellite-borne radar. This paper uses ground-based radar data and applies procedures similar to HC77 to determine the ensemble properties of the echo population described by a unique dataset obtained over the tropical western Pacific Ocean. At the Kwajalein Atoll, an S-band research radar has been operating since 1998 to collect data in support of the Tropical Rainfall Measuring Mission (TRMM) satellite (Schumacher and Houze 2000; Yuter et al. 2005; Houze et al. 2004). These radar data have excellent qualities, including high sensitivity, fine vertical and temporal resolution, and calibration matching with the TRMM satellite radar. An intensive field observation campaign, the Kwajalein Experiment (KWAJEX), supplemented the multiyear dataset for 23 July–15 September 1999. This study uses the data during KWAJEX to characterize the radar echo population in the vicinity of Kwajalein. In this study, we will examine the characteristics of the diverse Kwajalein echo population by examining data from a highly sensitive, continuously sampling, ground-based radar. In addition, we will compare the Kwajalein echo population with characteristics of the GATE radar echo population analyzed by HC77 to determine the similarities and differences between the two precipitating cloud populations and how differences in large-scale conditions may alter the basic characteristics of radar echo populations.

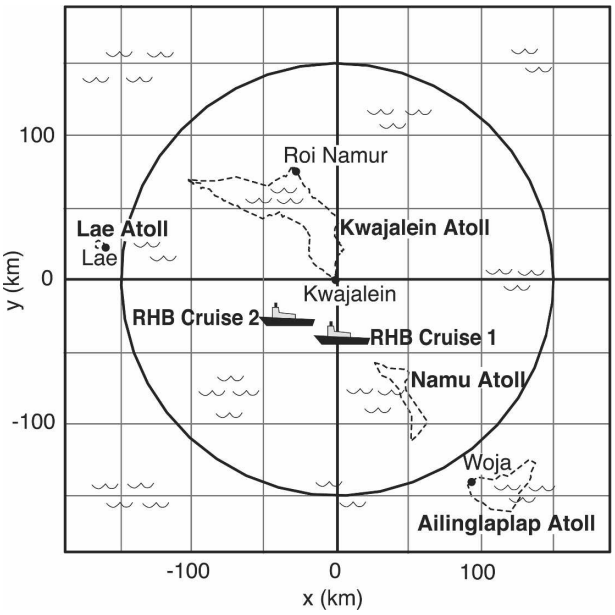

FIG. 1. Map of the KWAJEX study area. Dashed lines indicate edges of largely submerged coral atolls. Filled circles indicate sounding sites on the NOAA ship *Ronald H. Brown* (RHB) and at Kwajalein, Lae, Roi-Namur, and Woja atolls. The circle indicates a 150-km-radius range ring around the radar at Kwajalein.

2. Data and methods of analysis

a. Radar data

At intervals of approximately 12 min, the S-band Doppler Kwajalein radar (KR) provided a low pulse repetition frequency (PRF) surveillance scan (maximum range of 240 km) followed by two high PRF volume scans (maximum range of 150 km, see Fig. 1) consisting of 24 elevation angles (Yuter et al. 2005, hereafter Y05). For this study, the volume scan data were interpolated to a Cartesian grid with a 150 km × 150 km domain in the horizontal and 16 km in the vertical, and with 2 km × 2 km resolution in the horizontal, 1-km resolution in the vertical. For comparison, the radar data used in GATE analysis performed by HC77 was collected from a shipborne C-band radar, with a maximum range of 260 km. These data were not interpolated, and the analysis by HC77 was based on radar films from photographically recorded data of the radar plan position indicator (PPI) images. The KWAJEX data were digitally recorded and examined using the National Center for Atmospheric Research (NCAR) Zebra visualization software (Corbet et al. 1994), which allows on-demand inspection of arbitrary horizontal and vertical cross sections and a variety of data overlay choices.

Each radar echo detected in the low PRF surveillance scan (1° elevation angle) was analyzed during the KWAJEX time period. For this study, 13 days were chosen to sample a variety of rain events in order to represent the overall echo population at Kwajalein (Fig. 2). Although only 13 of the 55 days were sampled in this study, careful attention was paid to sample times that were representative of the overall KWAJEX population. The average and standard deviation of the percent echo area coverage for the 13 test days agree well with those during the entire KWAJEX time period. On most

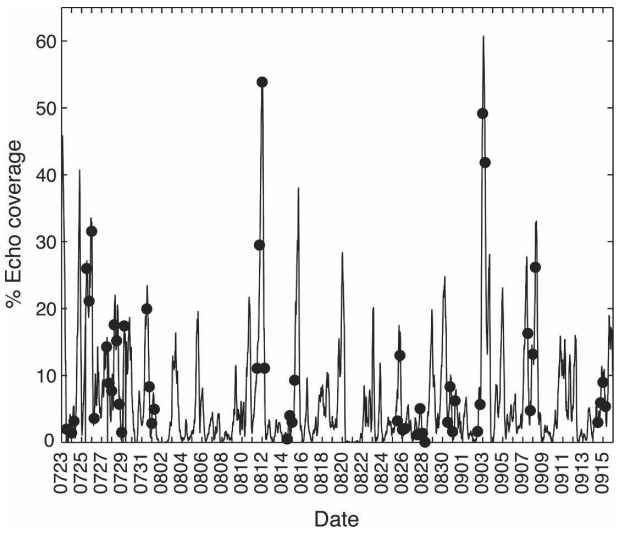

FIG. 2. Time series of the echo area coverage from the Kwajalein radar during KWAJEX. Dots indicate the echo area coverage for nominal analysis times included in this study.

of the sampled days, isolated convective echoes of small horizontal dimension were prevalent. However, three of the days included broad MCSs that moved through the KWAJEX domain (24–25 July, 11–12 August, and 2–3 September) and dominated the echo pattern.

On each of the selected days, nominal analysis times were 0000, 0600, 1200, and 1800 LST (1200, 1800, 0000, and 0600 UTC). A 15-dBZ echo intensity threshold defined an echo. Each echo present at a nominal time was identified and tagged. Altogether, 1200 echoes were tagged at the 52 nominal times. The characteristics of each tagged echo were determined in a manner similar to the analysis of the GATE echo population by HC77. The horizontal area of each identified echo was estimated by measuring a major and minor axis that, when multiplied, yield a rectangular area approximating the area covered by the echo. The height of the echo was measured by examining each height level of the interpolated volume scan in Zebra until the echo was no longer present, and the recorded height was the highest level that the echo was present. The 30-dBZ and minimum detectible echo heights were recorded. Because of the discrepancy between the ranges of the low PRF surveillance scan and the high PRF volume scan, several echoes had to be omitted from the height analysis because they lay outside of the domain of the volume scan. However, over 900 echoes were still within the bounds of the high PRF scan.

The morphology of each echo was further described in terms of 1) its orientation, and 2) the number and height of its convective cores. The orientation angle of the echo was determined by the angle of the major axis from a north–south line. We separated each echo into its convective and stratiform components. The convective–stratiform separation algorithm used was introduced by Churchill and Houze (1984) and later refined by Steiner et al. (1995) and Yuter and Houze (1997). The number of convective cores was determined, and the height of each was measured in a manner similar to the height of individual echoes described above.

We not only defined the static characteristics of the echoes at each nominal time, but also studied their life history. Each tagged echo was tracked both backward and forward in time on the low PRF surveillance scan (as in HC77, but using the method of Williams and Houze 1987), with a 12-min. temporal resolution, as provided by the scan strategy. Each echo was tracked to its formation and dissipation times to determine its modes of formation and dissipation, duration, speed, and direction of motion. The formation and dissipation modes were identified as either independent (forming by simply appearing or dissipating by disappearing), or as a result of an echo merger or split. Echoes that formed or dissipated outside of the region of radar coverage accounted for less than 5% of all echoes, and were omitted in the lifetime analyses. Velocity (speed and direction) of echo motion was determined by measuring the displacement of the echo from its formation point to its dissipation point and dividing by its time of travel between those two points.

Since MCSs occurred infrequently, the KWAJEX time period did not contain a representative sample of these large features. We therefore examined a longer period of data to obtain a larger sample of MCSs. For this purpose, we considered KR data from July 1999 to December 2000. An MCS was considered to be an echo over 100 km in horizontal dimension at some point in its lifetime and in view of the radar for at least 2 h (the range of durations was 2–8 h).

b. Sounding data

Upper-air soundings were launched from five stations that formed a closed array around the KWAJEX study area (Fig. 1): the islands of Kwajalein, Roi-Namur, Lae, Woja, as well as the National Oceanic and Atmospheric Administration (NOAA) ship *Ronald H. Brown* (Y05). Sobel et al. (2004) applied a comprehensive quality control and averaging procedure to all of the soundings. The result was a time series of regionally averaged soundings with a time resolution of 3–6 h. Small-scale local fluctuations were filtered out by this procedure.

The composite sounding data were used to relate the observed radar echo characteristics to the environmental thermodynamic structure and winds. In general,

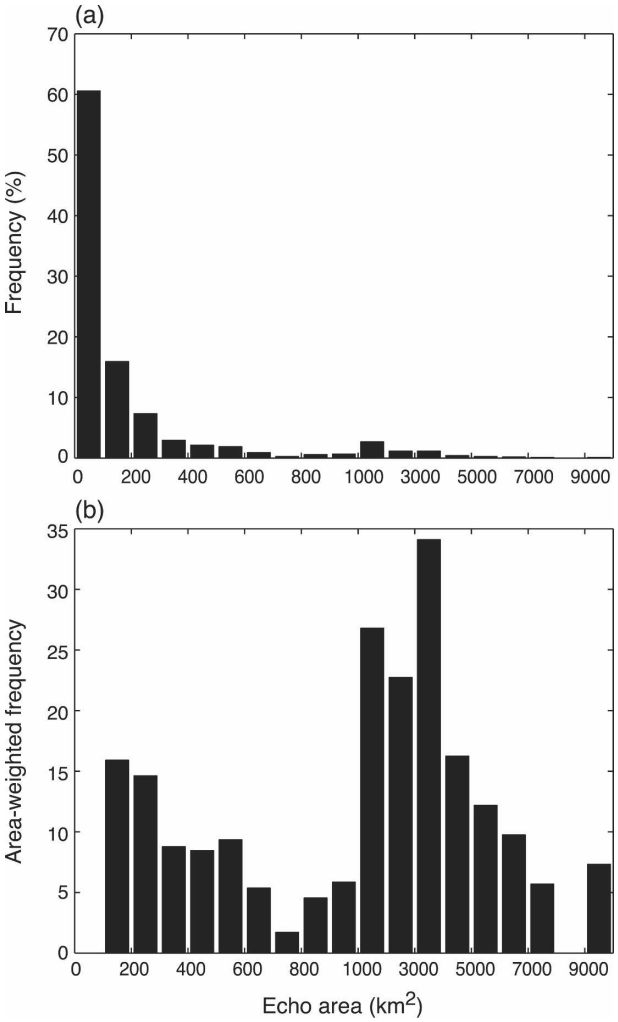

FIG. 3. Frequency distribution of the area of radar echoes observed during KWAJEX: (a) number and (b) area distribution. The height of a bar indicates the number of echoes in a given size category.

composite sounding data were available within 1 h of each of the nominal times, and if that time threshold was exceeded, the comparison was not performed. Of the 52 analysis times, 45 had composite sounding data available to perform the comparison.

3. Characteristics of the average KWAJEX echo population

a. Echo area

The numerical dominance of the small-scale convection during KWAJEX is illustrated by the frequency distribution of echo area in Fig. 3a. Most of the echoes are small (<300 km^2). However, the area-weighted frequency in Fig. 3b shows that the few echoes in the tail of the number distribution account for the majority of area covered by echoes.

The accumulated frequency distribution of echo size is shown in log-probability format in Fig. 4 for KWAJEX and GATE. Exact comparison of the two echo populations is complicated by the differences in the instrumentation used in the experiments. Although both datasets were obtained with well-calibrated radars (Hudlow 1979; Hudlow et al. 1979; Y05; Houze et al. 2004), the R/V *Oceanographer* radar used in the study by HC77 was less sensitive than the KR. However, because the differences in the distribution owing to the lesser sensitivity of the GATE radar should be systematic, the trends of both radars can be compared.

In the log-probability format used in Fig. 4, a straight line indicates a lognormal distribution. The areas for KWAJEX and GATE exhibit nearly lognormal distributions, except for the largest 0.1% of echoes. Other studies of the area distributions of convective radar echo populations have noted that the populations tend to be lognormally distributed (López 1977, hereafter referred to as L77; HC77; Y05). L76 and L77 suggested that the lognormality of a convective echo population arises from the fact that entrainment and other processes lend randomness to the potential of a cloud element to grow from one size to the next. He pointed out that in general a lognormal distribution is the result of a multiplicative random process in which a step in the growth of an echo is a random proportion of its previous size.

The deviation from lognormal of the largest echoes seen in Fig. 4 for both GATE and KWAJEX is characteristic of a truncated lognormal distribution. The truncation will occur at the size above which the rain areas cannot exist because of either physical or dynami-

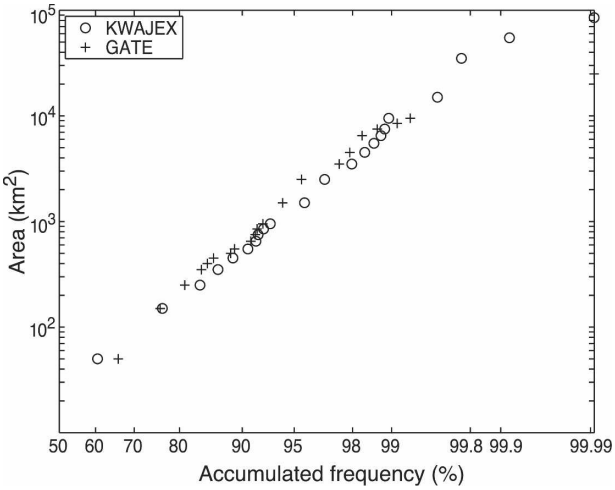

FIG. 4. Accumulated frequency distribution of areas covered by KWAJEX and GATE radar echoes plotted in log-probability format.

cal restrictions on their horizontal scale. In this case, the truncation may be produced by observational limitations since the radar's field of view is limited to a maximum range of 240 km. The KWAJEX and GATE distributions are similar through their truncation points; however, the GATE echoes truncate for smaller areas than the KWAJEX echoes.

b. Echo height

The echo-top height was determined for each of the tagged echoes in two ways. First, we used the minimum detectable (MD) signal to determine the absolute maximum indicated height. Second, since the MD signal is range dependent, we also determined the maximum height of the 30-dBZ contour since these values are range corrected. The resulting frequency distributions are plotted in Fig. 5a, along with the GATE echo height distribution. The distribution of MD height for the KWAJEX echoes shows that there is a maximum at approximately 7 km, and a weak (statistically insignificant) secondary maximum at 9 km. Although the results of Schumacher and Houze (2003b) indicate frequent shallow isolated rain cells from a satellite perspective, extremely shallow cells do not produce a separate peak in the distribution in Fig. 5. The lack of a peak associated with extremely shallow clouds could be because either 1) most of the shallow cells contain only small (drizzle sized) drops, and our echo threshold of 15 dBZ prevents us from characterizing cells composed of such small precipitation particles, or 2) the radar beam at far ranges was above the echoes, thus not sampling them.

Comparing the results to the GATE dataset, we see that a weak secondary peak exists for the GATE echoes as well, though it too is statistically insignificant. Overall, the heights are lower in GATE than in KWAJEX. HC77 found an average maximum echo height of 4.8 km, whereas the average height for the KWAJEX echoes was 7.2 km for the MD threshold. These differences could be due to the lower sensitivity of the *Oceanographer* radar compared to Kwajalein. However, even when the threshold of the KWAJEX echo heights was increased to 30 dBZ (see Fig. 5a), the smallest KWAJEX echoes were still shifted toward greater heights. Since it is highly unlikely that the *Oceanographer* radar was so insensitive that its MD echo exceeded 30 dBZ (Hudlow 1979; Hudlow et al. 1979), the KWAJEX echoes do appear to have higher average heights than those in the GATE area. Differences in the cloud-top temperatures between GATE and KWAJEX also suggest that the difference in the heights is real. Average cloud-top temperatures in the vicinity of Kwajalein are approximately 11° colder than

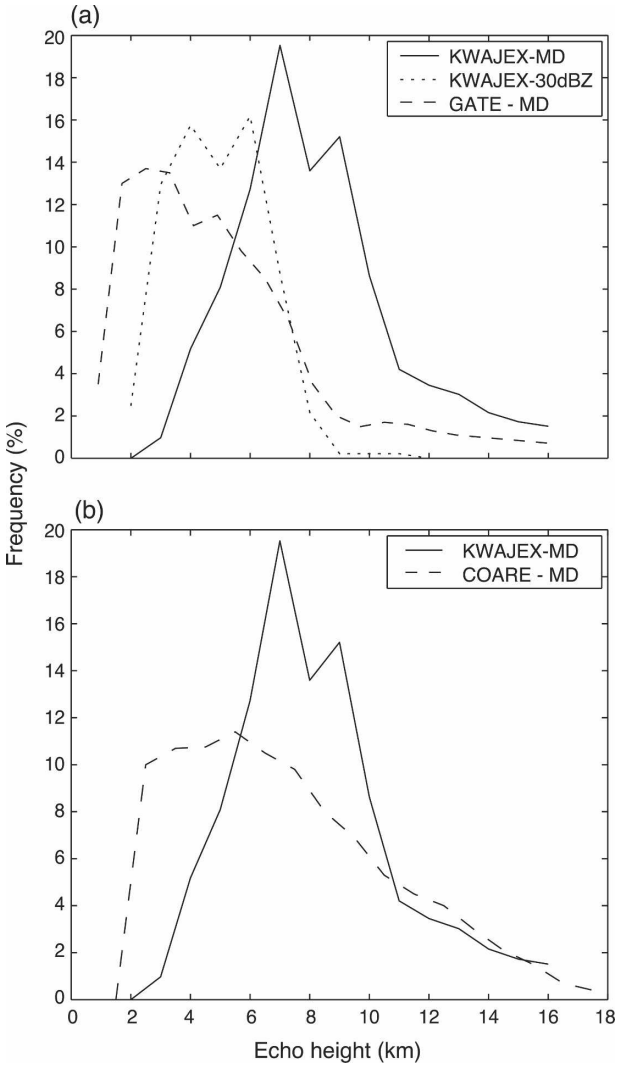

FIG. 5. (a) Frequency distribution of the minimum detectible and 30-dBZ radar echo heights observed during KWAJEX and the minimum detectible radar echo heights observed during GATE. (b) Same as in (a), but also the minimum detectible radar echo heights of convective elements observed during TOGA COARE by Rickenbach and Rutledge (1998).

GATE [251.7 and 262.5 K, respectively; cloud-top temperatures were determined using the International Satellite Cloud Climatology Project (ISCCP) satellite observations; Rossow et al. 1996].

To better understand the factors determining the difference in echo heights between KWAJEX and GATE, average soundings of temperature, relative humidity, and equivalent potential temperature for the study periods of the two research projects are plotted in Fig. 6. Figure 6a shows that between 500 and 400 hPa, there is a sharp decrease in dewpoint temperature in the GATE sounding. This difference is clearly evident in the vertical distribution of GATE relative humidity of the two

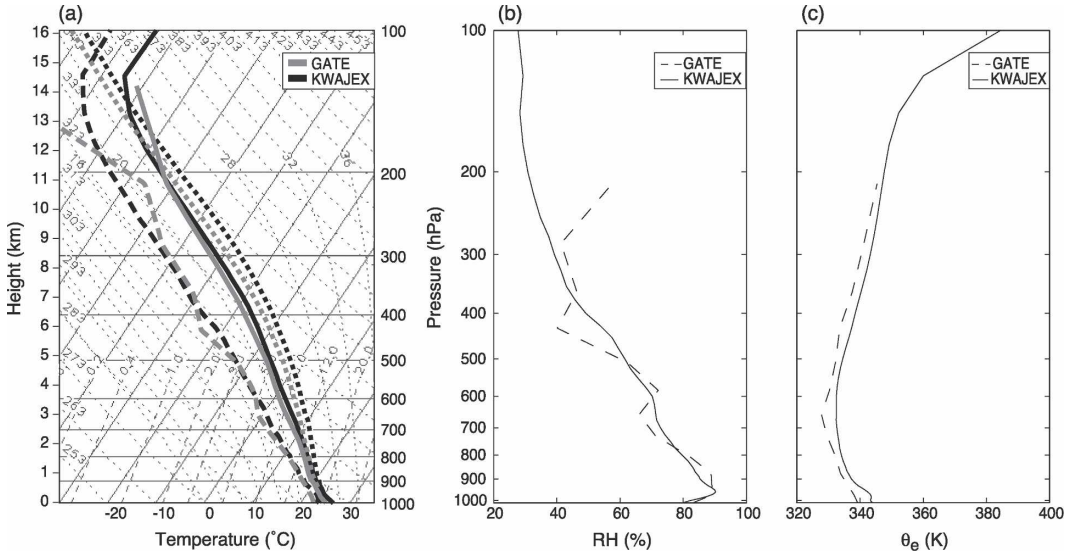

FIG. 6. (a) Average thermodynamic soundings for the entire KWAJEX and GATE experiments. Temperatures are indicated by the heavy solid line, dewpoint temperatures by the heavy dashed line, and temperatures of lifted surface parcels by the dotted line. (b) Relative humidity and (c) equivalent potential temperature profiles for KWAJEX and GATE as derived from the soundings in (a).

projects in Fig. 6b. The humidity is up to 20% lower in midlevels than in KWAJEX. This difference would be expected to limit the height of the GATE echoes. The lower humidity in midlevels in GATE is consistent with midlevel influx of dry Saharan air intruding into the GATE study region (Carlson and Prospero 1972; Dunion and Velden 2004). Additionally, the profiles of equivalent potential temperature (Fig. 6c) show that θ_e is consistently higher at all levels in KWAJEX compared to GATE. Comparing the convective available potential energy (CAPE) and convective inhibition (CIN) for the two soundings in Fig. 6a, we find the KWAJEX sounding had more CAPE than GATE (2248 compared to 1414 J kg^{-1}) and similar CIN (-2.9 and -2.2 J kg^{-1}, respectively). These factors suggest that the KWAJEX environment had more potential for deep convection than GATE, consistent with the observed taller echoes for KWAJEX.

Rickenbach and Rutledge (1998) determined the frequency distribution of convective feature heights for radar echoes analyzed during the Tropical Ocean Global Atmosphere Coupled Ocean–Atmosphere Response Experiment (TOGA COARE), which was conducted over the western Pacific warm pool. Figure 5b shows the distribution of the KWAJEX and TOGA COARE echo heights. Although the two distributions have similar mean values (approximately 7.2 km), the distributions are somewhat dissimilar. The two distributions exhibit a similar trend for the largest echoes; however TOGA COARE has a peak at the smallest echo heights, while the KWAJEX distribution peaks in the middle heights as described above. Rickenbach and Rutledge (1998) applied no reflectivity threshold to the TOGA COARE echoes. That method would lead to recording of higher echo tops for strong convective cells, but at the same time it would be more likely to capture small cells composed of drizzle-sized drops that would fall below the 15-dBZ threshold used in our KWAJEX analysis. If such weak cells were numerous, the TOGA COARE distribution would be shifted toward lower echo-top heights compared to KWAJEX.

When plotted in log-probability format, the distribution of MD echo height approximates a straight line indicative of a lognormal distribution (Fig. 7). This lognormality only deviates significantly for echoes above 14 km. L77 and HC77 also noted truncation of the echo height distribution and attributed it to the fact that heights are limited to the height of the tropopause, which is at approximately 15 km in the Kwajalein and GATE regions. Evidence of the secondary maximum at 6–9-km height is also evident in this plot in the form of a slight deviation from a straight line at these heights. Figure 7 shows the frequency distribution of GATE echo maximum heights for comparison. We see that although the two distributions are approximately lognormal, and that they truncate at the same height, the slope and mean of the two are noticeably different, indicating the systematically lower echo tops in GATE.

Mean heights of the KWAJEX echoes were positively correlated with area, with the increase being al-

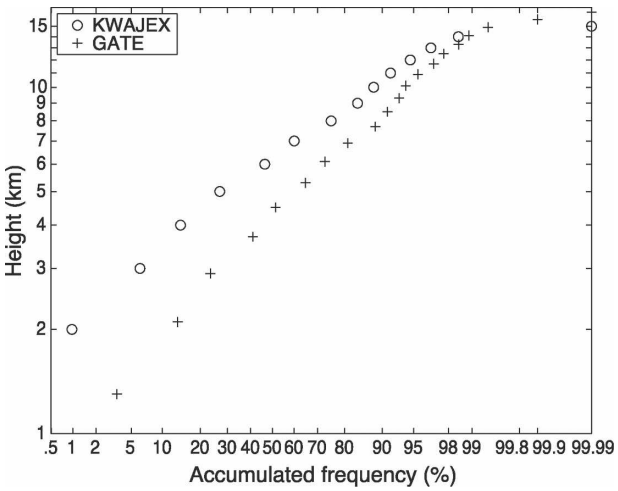

FIG. 7. Accumulated frequency distribution of the minimum detectible radar echo heights observed during KWAJEX and GATE plotted in log-probability format.

most linear with area plotted in log format (Fig. 8a). The KWAJEX and GATE echoes follow a similar trend, with the mean heights being positively correlated with echo area, except that the KWAJEX echoes are in general taller, consistent with the findings in Fig. 5a. Despite the systematic trend of mean height and area, the spread of values is extreme, as indicated by the scatterplot in Fig. 8b. Echoes of a given horizontal dimension exhibit a wide range of heights, depending on their stage of development and random variations in environmental conditions.

As a result of entrainment, the environmental humidity and buoyancy influence the maximum height reachable by convective clouds (e.g., Houze 1993, chapter 7). Each sample time was categorized according to whether the majority of echoes were shallow (average heights <4 km), of medium height (average heights 4–10 km), or deep (average heights >10 km). The composite soundings were averaged for these three categories (Fig. 9). The temperature profiles (solid lines) for each category are nearly identical, as are the buoyancy (dotted lines) of boundary layer parcels. These properties are also evident in the profiles of potential temperatures (Fig. 10b), which show the θ curves to be almost identical. The values of CAPE for the three are similar (but increasing) for the shallow, medium, and deep echoes (2039, 2149, and 2499 J kg^{-1}, respectively), with deeper echoes existing in conditions of more convective potential energy.

The humidity characteristics of the three echo height categories exhibit stronger differences. The dewpoint temperature profiles (dashed curves in Fig. 9) show two humidity minima (550–450 and 400–300 hPa) for shallow echoes. For echoes of medium height (Fig. 9b), the lower humidity minimum is absent, while the upper humidity minimum remains unchanged. The sounding corresponding to cases of deep echo (Fig. 9c) shows moistening through the entire depth of the troposphere, with dissolution of both relative humidity minima. This result is further highlighted in Fig. 10. The dry air in midlevels in the shallow echo category produces a much more pronounced minimum of θ_e in midlevels than in the deep-cell cases. However, below the 800-hPa level, the conditional instability is greater in the deep-cell cases. The surface value of θ_e is greater, and the drop-off of θ_e with height is more rapid than in the shallow cases. The greater echo heights may arise from this stability difference, while the more moist midlevels may decrease the inhibiting effect of entrainment, so that cells can attain greater heights. But, as is usually the case, we cannot rule out here that the higher

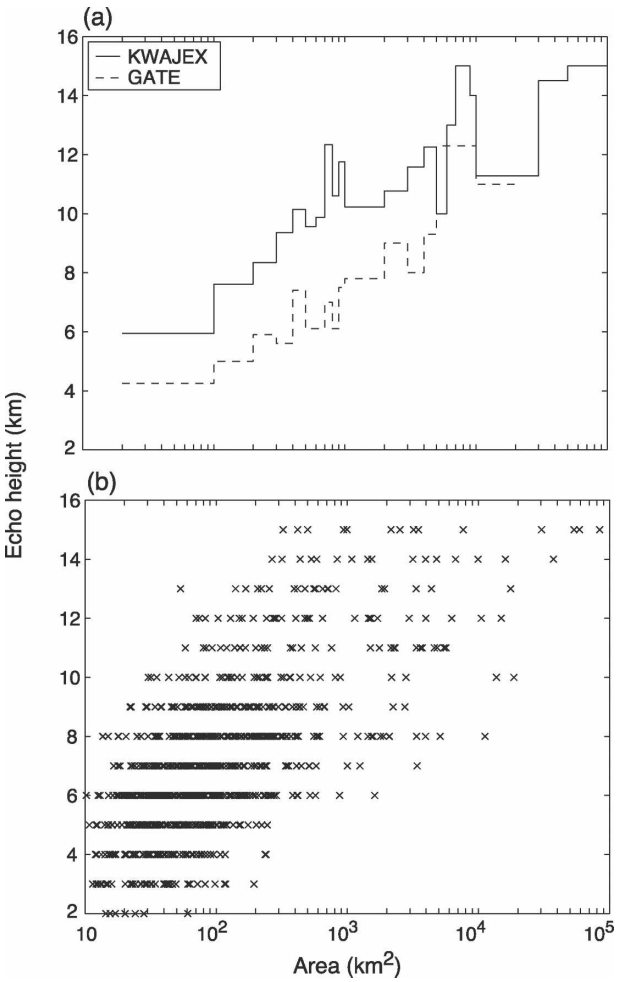

FIG. 8. (a) Average minimum detectible radar echo heights observed during KWAJEX and GATE in different size ranges. (b) Scatterplot of KWAJEX radar echo.

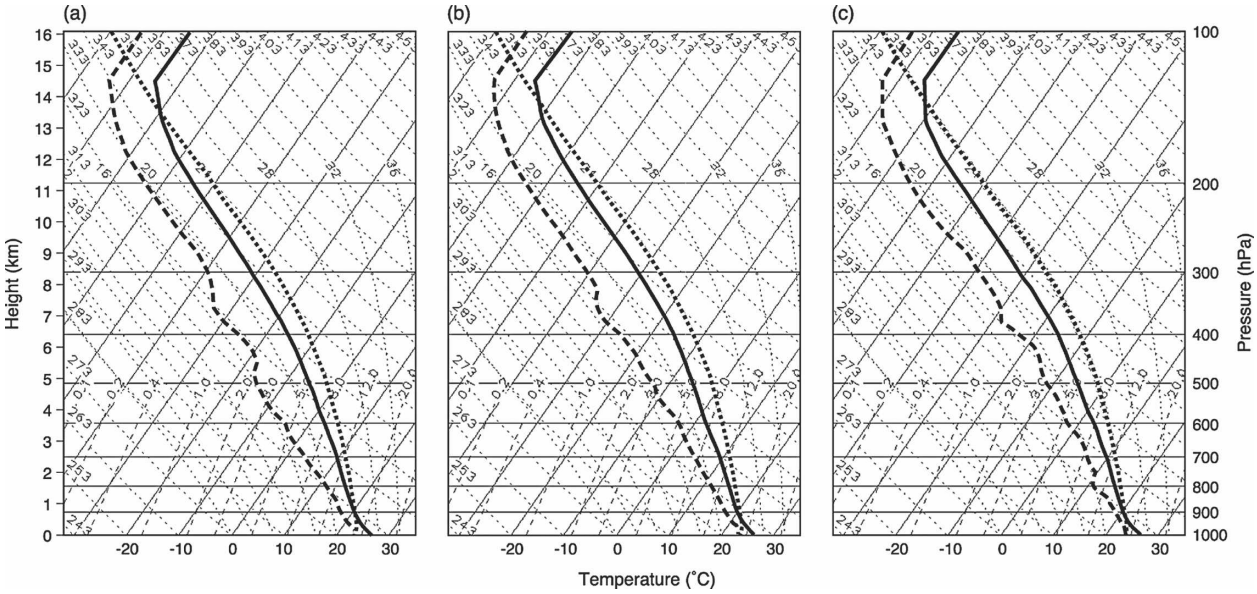

FIG. 9. Average thermodynamic soundings for times of (a) shallow echoes (average heights <4 km), (b) medium echoes (average heights 4–10 km), and (c) deep echoes (average heights >10 km). Temperatures are indicated by the heavy solid line, dewpoint temperatures by the heavy dashed line, and temperatures of lifted surface parcels by the dotted line.

humidity and θ_e in midlevels in the deep-cell cases is an effect rather than a cause of the deeper convection.

c. *Echo formation, dissipation, and duration*

After the instantaneous descriptors for each echo were measured for each analyzed radar scan, the echoes were tracked throughout their lifetimes, and their formation and dissipation modes were determined. Small echoes were more likely to form and dissipate independently, while mergers and splits bounded the lifetimes of the medium and large echoes (Figs. 11a,b). Merging and splitting were also found to be common in the western Atlantic (L76) and GATE (HC77) echoes, but they are more prevalent at Kwajalein. The formation and dissipation modes of both KWAJEX and GATE echoes are compared side by side in Fig. 11. For all sizes, the lifetime of the KWAJEX echoes is more likely to be bounded by merging or splitting than the GATE echoes. Apparently, the Kwajalein region was more crowded with echoes than GATE during these field campaigns, possibly as a result of the greater sea surface temperature in the vicinity of Kwajalein than in the GATE region.

As with the distributions of echo area and height, L77 found that durations also follow a lognormal distribution, which he suggested was a result of the cloud population following a law of proportionate effects. The accumulated frequency distributions of duration of KWAJEX and GATE echoes are plotted in log-probability format in Fig. 12. The distributions of duration do not form as straight a line as the distributions of area (Fig. 4) and height (Fig. 7). The middle range of lifetimes appears to follow a straight line. However, the truncations of lifetime by merging and splitting produce a deviation from lognormality at longer lifetimes (>~300 min). The truncations generally prevent extremely long-lived echoes. The log-probability curve for echo durations also deviates from lognormality at shorter lifetimes (<~24 min), where the curve recedes from the straighter midsection. This effect is produced by the rather long time interval (~12 min) between observations. In general, the KWAJEX echoes have shorter lifetimes than those of GATE (averages of 72 and 88 min, respectively). The shorter lifetimes of the KWAJEX echoes are consistent with the above finding that the lifetimes of KWAJEX echoes tend to be more frequently bounded by mergers and splits than GATE.

The average duration of the KWAJEX echoes of different sizes is plotted as a function of mean echo area in Fig. 13a. Mean echo duration and area do not correlate for echoes <8000 km^2. However, the largest echoes (most of which are the MCSs) do seem to have longer lifetimes. Other studies of tropical radar echo populations indicate a more general positive correlation between echo area and duration (i.e., Iwanchuk 1973; L76; HC77). However, at Kwajalein, the larger the echo, the more likely its lifetime will be bounded by mergers/splits. This effect is strong enough to eliminate any correlation between area and duration for all but the very long-lived MCSs. Figure 13b plots the area

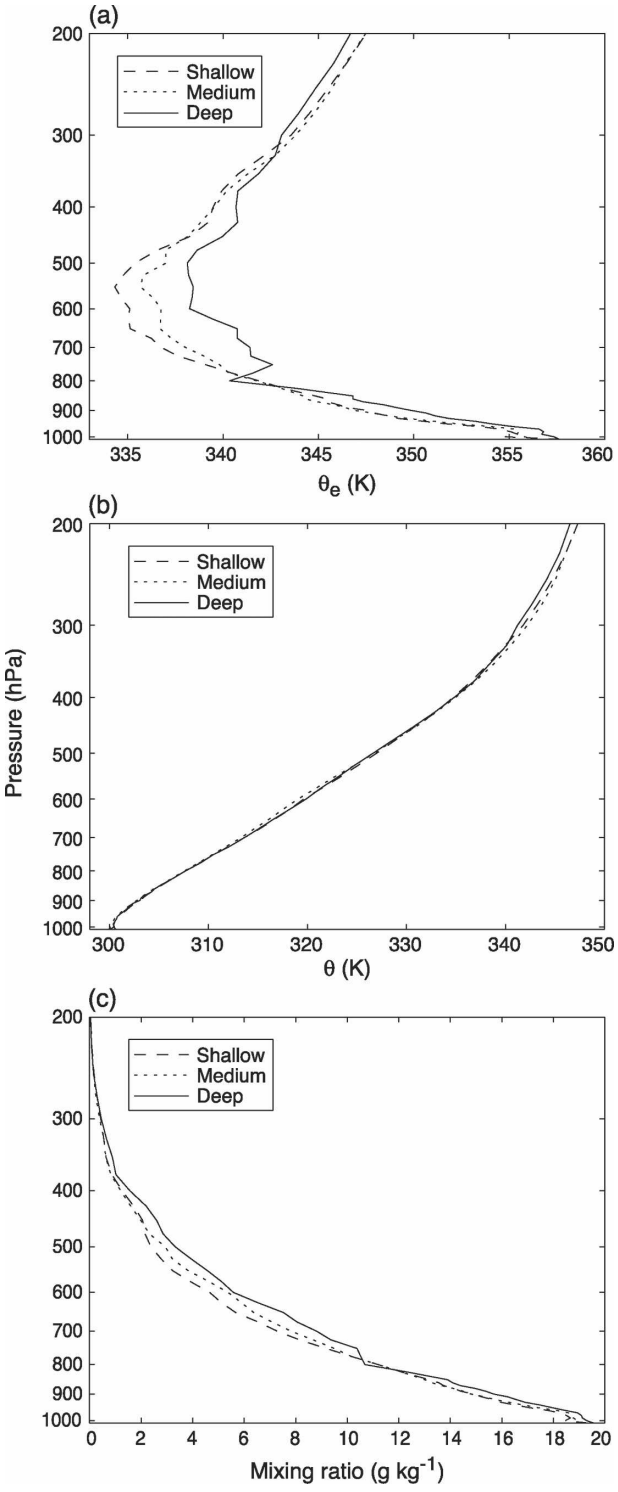

FIG. 10. Vertical profiles of (a) equivalent potential temperature, (b) potential temperature, and (c) mixing ratio for times of shallow echoes (dashed), medium echoes (dotted), and deep echoes (solid) as derived from the thermodynamic soundings in Fig. 9.

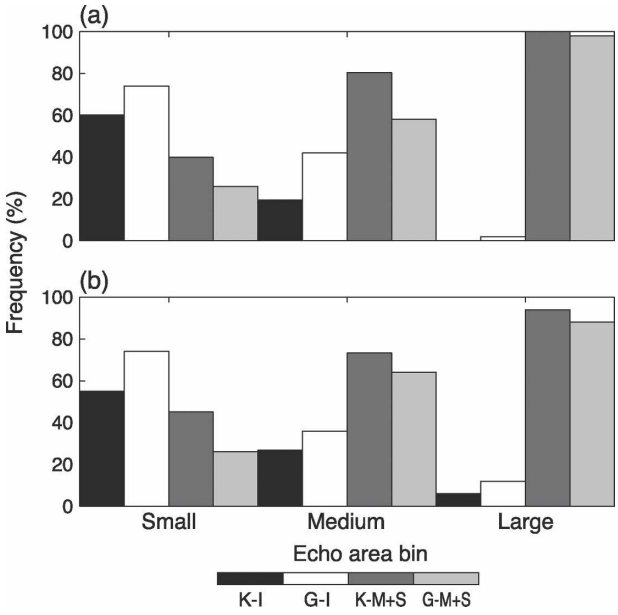

FIG. 11. Histograms of the frequency of independent (I) and merging and splitting (M + S) modes of (a) echo formation and (b) echo dissipation observed during KWAJEX (K) and GATE (G).

versus height distribution in scatter form. The weak correlation between area and height is apparent with slightly longer durations for larger areas. The spread is similar for all areas, which can be a difference of 300%. It is therefore difficult to parameterize duration for any given area because any echo can have a large range of lifetimes.

d. Echo motion

Figure 14a displays the average speed of motion as a function of echo size. Overall the speeds are highly

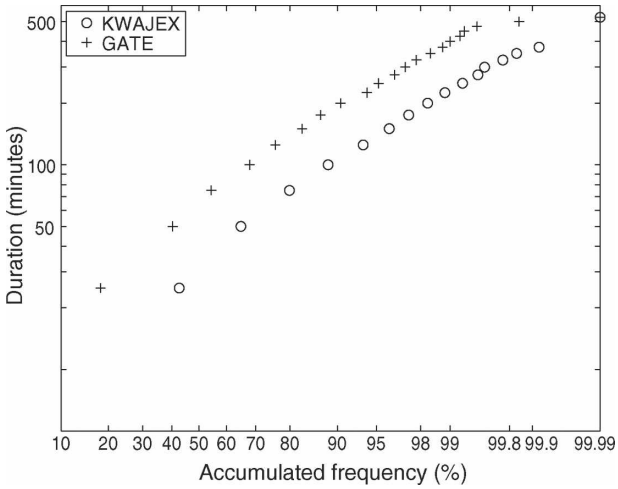

FIG. 12. Accumulated frequency distribution of KWAJEX and GATE radar echo durations plotted in log-probability format.

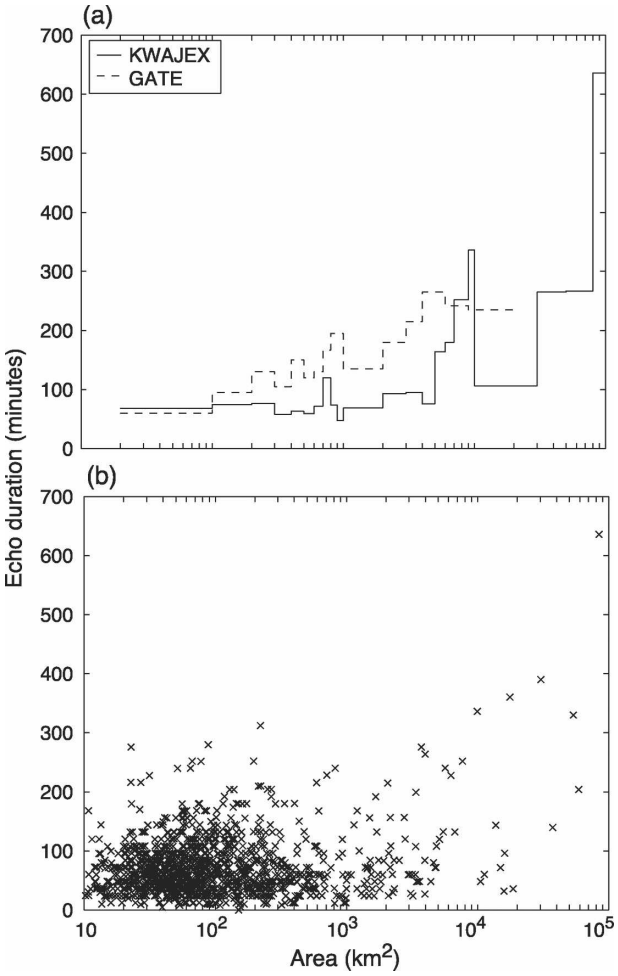

FIG. 13. (a) Average radar echo durations observed during KWAJEX and GATE in different size ranges. (b) Scatterplot of KWAJEX radar echo.

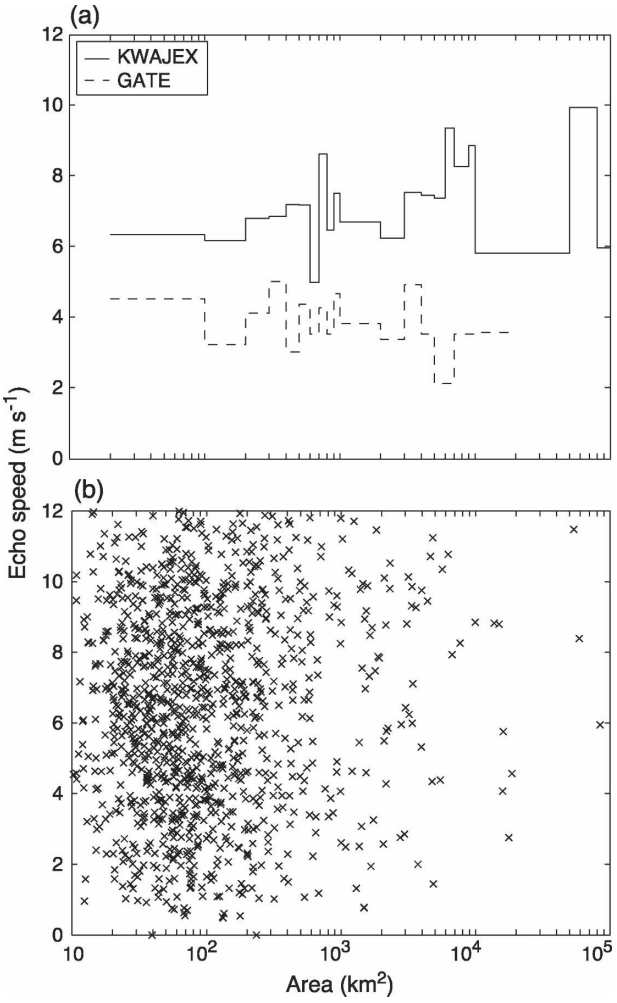

FIG. 14. (a) Average speeds of radar echoes observed during KWAJEX and GATE in different size ranges. (b) Scatterplot of KWAJEX radar echo.

variable. Squall-line echoes were omitted from this plot because they were small in sample, and their speeds (generally 12–18 m s^{-1}) were not representative of the rest of the population. The average echo speed was 6.4 m s^{-1}. HC77 found no correlation between non-squall echo speed and area, and their average speeds were much slower (3–5 m s^{-1}). Figure 14b indicates that any echo size can move at any number of speeds, likely due to changing wind speeds in the region.

Figure 15 shows that the majority of the echoes in the Kwajalein region moved east to west (~100° from north). These echo track angles correspond closely to the 900–600-hPa wind direction. In general, very little directional wind shear existed in the 900–600-hPa level in the KWAJEX domain; however, the correspondence between the 700-hPa wind direction and the echo track angles is the closest (Fig. 16). The difference between the 700-hPa wind direction and the echo track angle shows that nearly all of the KWAJEX echoes moved within 45° of the 700-hPa wind direction, with many tracking nearly exactly. HC77 reported that most of the GATE echoes were advected by the 850-hPa winds. The difference in the levels of advection is consistent with the result that, in general, KWAJEX echoes have greater heights than GATE echoes; therefore, the level that the echoes would track best with would be at a higher altitude (lower pressure) for echoes at Kwajalein.

e. Echo orientation

Echoes that had a major-to-minor axis ratio >1.5 were deemed sufficiently elongated to assign an orientation, and that orientation was determined by the major axis. The average axis ratio was 2.4, and 83% of the

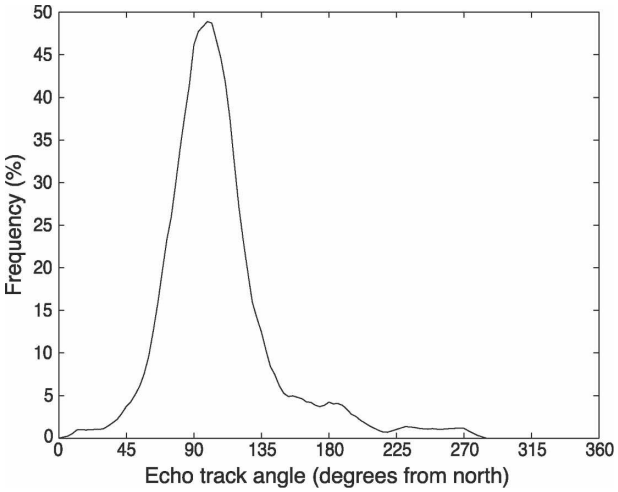

FIG. 15. Frequency distribution of the average track angle the KWAJEX radar echoes followed during their lifetimes. Angles were measured in degrees from north (clockwise).

KWAJEX echoes satisfied the 1.5 axis ratio threshold. That is, nearly all echoes showed a tendency to form lines. From Fig. 17, it is evident that the distribution of echo orientations is bimodal, with a strong tendency for the KWAJEX echoes to be aligned in either a northeast–southwest (~45°) or a northwest–southeast (~−45°) orientation. We tested the sensitivity of this result to the axis ratio chosen to define an elongated echo. The strong bimodal distribution peaking at the same two orientations seen in Fig. 17 was also observed for more elongated echoes (e.g., major-to-minor axis ratios of 3:1 and 5:1).

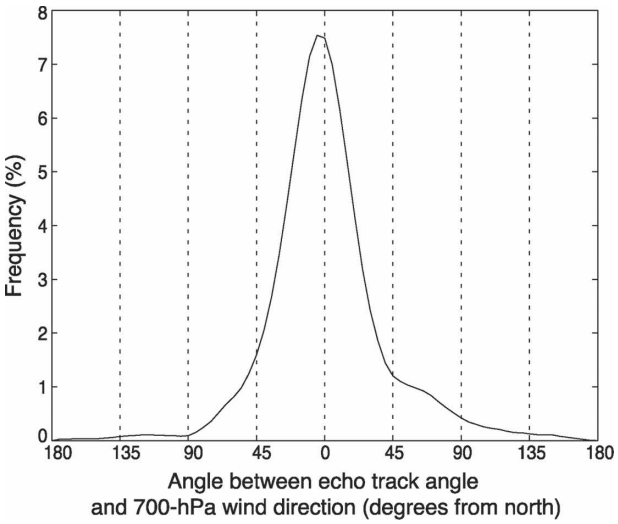

FIG. 16. Frequency distribution of the difference between the KWAJEX radar echo track angle and the 700-hPa wind direction.

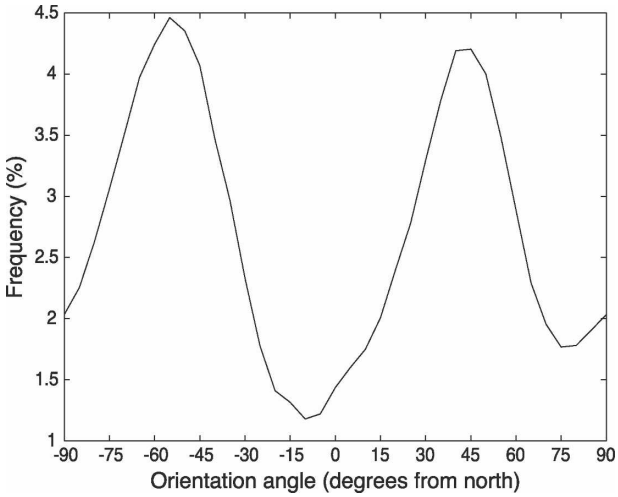

FIG. 17. Frequency distribution of the radar echo orientation angles observed during KWAJEX. Orientation angles were measured by the smallest angle between true north and the orientation, with values ranging from −90° to +90°. Positive angles were clockwise from north; negative angles were counterclockwise from north.

To examine these modes in relation to the wind field over the KWAJEX region, the echo orientations were compared to the low-level shear vector (LLSV; defined as the wind shear between the 1000–800-hPa levels in the composite sounding data). Figure 18 is a histogram

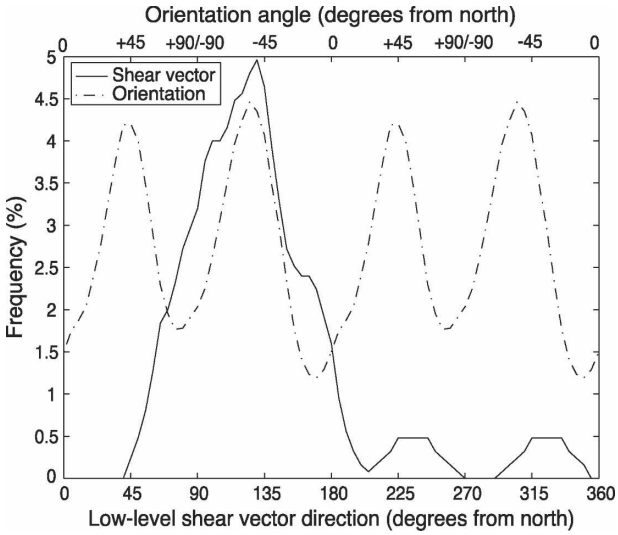

FIG. 18. Frequency distributions of both the low-level shear vector direction and the radar orientation angles observed during KWAJEX. The low-level shear vector was described by the 1000–800-hPa shear vector. Orientation angles were repeated to cover the range of angles between 0° and 360° for comparison with the shear vector. The axis of the corresponding orientation angles is at the top of the figure for reference.

of both the orientation angles and the direction of the LLSV. The histogram of orientation angles was repeated to represent the entire 360° circle (because orientation is not a vector, a +60° oriented echo is the same as a −120° oriented echo). There is a strong tendency for the LLSV to be oriented in an easterly or east-southeasterly direction. When compared to the orientation angles, it is apparent that −45° oriented echoes tend to be parallel to the LLSV (as denoted by coincident maxima in the histograms). Likewise, we see that there is a 90° offset between the +45° oriented echoes and the maximum in the LLSV direction, indicating that these echoes tend to be oriented perpendicular to the LLSV.

This result is a statistical verification of the shear-parallel and shear-normal modes of convective line organization that has been seen over tropical oceans in the GATE area and over the western Pacific warm pool (Barnes and Sieckman 1984; LeMone et al. 1998; Johnson et al. 2005). These previous studies found that shear-normal echo lines had propagation speeds that were considerably faster than the shear-parallel lines (generally more than twice as fast). However, the shear-parallel and shear-normal echoes observed during KWAJEX had similar speeds. Indeed, we found little difference between the two modes with respect to any echo characteristic. Only for very elongated echoes (5:1 major to minor axis ratio) do the two modes exhibit a noticeable difference in speeds (6.2 m s^{-1} for the shear-parallel mode and 8.6 m s^{-1} for the shear normal-mode); however, echoes of this degree of elongation were extremely rare. The greater speeds for the shear-normal lines are consistent with the previous studies mentioned above; but, the magnitude of the difference in speeds is not nearly as large at Kwajalein compared to the other studies. We suspect that the difference in speed between shear-parallel and shear-normal lines in KWAJEX was masked by the strong trade winds in the Kwajalein region. The difference between the speed of motion of the two types of line modes may result from a discrete propagation component that enhances the net speed (resulting from advective plus discrete components of motion) of the shear-normal lines. If the advective component of the wind is particularly strong it will dominate the motion.

The percentages of the shear-parallel and shear-normal echoes present for each sample time are plotted in Fig. 19. At any given time, at least one of the modes is present, accounting for 15%–100% of all echoes present. Figure 19 demonstrates that the shear-parallel and shear-normal modes can appear simultaneously and with almost equal frequency. The coexistence of the shear-parallel and shear-normal modes within the region of radar observation indicates a potential difficulty in parameterizing line orientation in terms of large-scale variables.

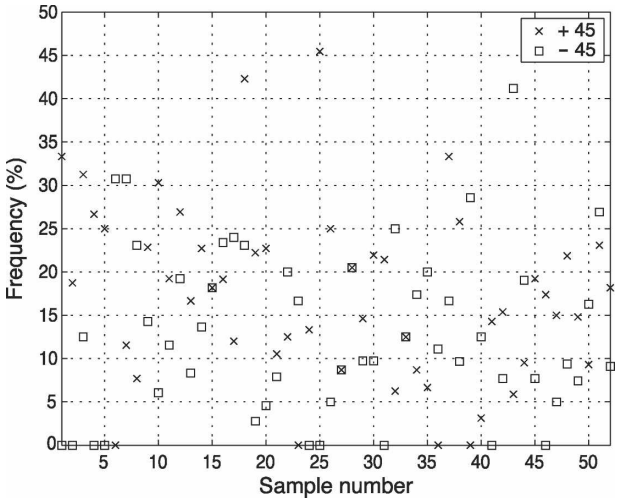

FIG. 19. Frequency of occurrence of the two dominant orientation angle modes observed during KWAJEX for each test time in this study. Each test time during the study is indicated by the sample number (1–52). The frequency of occurrence of the modes was determined by counting the total number of echoes with orientations within ±10° of the mode.

f. Echo internal structure

To determine the extent to which large precipitating clouds in KWAJEX contained cores of intense convection and rainfall, we applied the convective–stratiform separation algorithm discussed in section 2, and then counted the number of cores identified within each echo. Figure 20 shows that, in general, echoes >400 km^2 have multiple convective echo cores. The trend of the plot shows an increase in the number of embedded convective cores as the area of the echo increases, a result also seen in the GATE echoes by HC77. The differences in the number of convective cores between the GATE and KWAJEX populations are likely affected by differences in the sampling strategy. The KWAJEX convective cores were determined by an advanced convective–stratiform separation algorithm (section 2a), whereas a GATE convective core was defined by a reflectivity threshold of 31 dB*Z*. Additionally, the beamwidth of the *Oceanographer* radar used in the HC77 study was 1.5°, which could effectively merge two convective cores that were in close proximity to one another (the beamwidth of the radar used in this study was 1.12°; see Y05 for details). It should be noted that although the average number of convective cores increases slightly with increasing area, the percentage of area covered by convective rain decreases sharply.

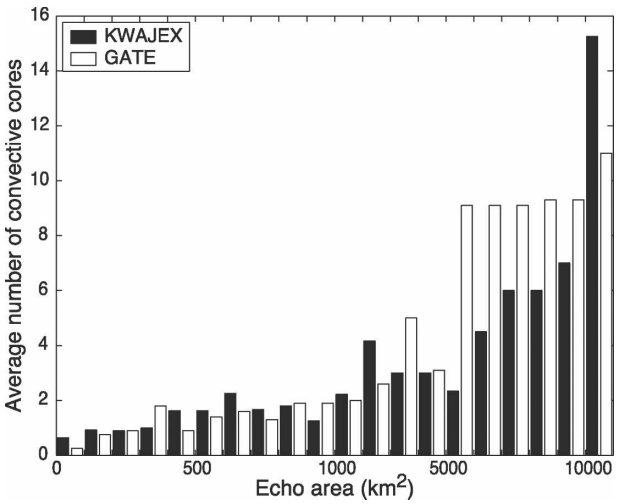

FIG. 20. Average number of embedded convective cores located within KWAJEX radar echoes, and number of embedded cores of maximum radar reflectivity located within GATE radar echoes in different size ranges.

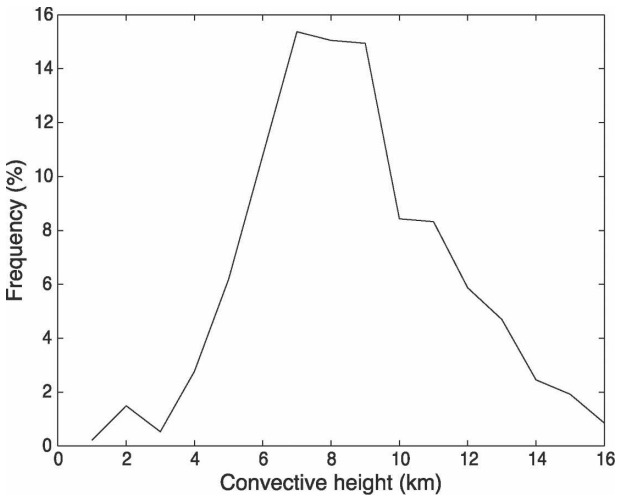

FIG. 21. Frequency distribution of the minimum detectible heights of the convective cores observed during KWAJEX. Convective cores were identified by applying a convective–stratiform separation on the radar data.

Houze (1993) noted that in the extreme case of a mature tropical MCS, only ~10% of the rain area is considered to be actively convective, the remainder being stratiform. Similarly at Kwajalein, the greater the area of an echo, the greater the percentage of stratiform rain area.

Johnson et al. (1999) found evidence of three separate stable layers in soundings from GATE and the western Pacific and suggested that these stable layers were associated with a "trimodal" distribution of convective feature heights. They used not only radar data but photographic data of the visible clouds, not necessarily seen by radar, during TOGA COARE to provide evidence of the existence of clouds of three different categories: *shallow cumulus*, *cumulus congestus*, and *cumulonimbus*. The existence of clouds in these size categories, of course, does not prove spectral peaks existed in echo or cloud heights corresponding to these three cloud types. Instead, they hypothesized that these three cloud types were associated with the three stable layers in the soundings, which were near 2 km, at the 0°C level (near 5 km), and at the tropopause (15–16 km).

To further examine the height distribution in KWAJEX, we determined the echo-top height for each of the regions identified as convective by the convective–stratiform algorithm. Figure 21 shows the frequency distribution of these heights. These echo heights differ from those in Figs. 5–9, which analyze the overall height of the echo, since Fig. 21 refers to the height of individual convective elements within the echoes. Figure 21 exhibits one distinct modal peak, at 7–9 km. However, we note a small (statistically insignificant) maximum in the frequency of echo heights in the 1–3-km range, followed by a sharp increase in frequency from 3 to 7 km, up to the main modal peak at 7–9 km, followed by a decrease in frequency from 9- to 16-km echo height. The drop-off in the frequency of convective feature heights between 10 and 16 km is less drastic than the increase from 3 to 7 km (similar features were found in TOGA COARE radar echoes by Rickenbach and Rutledge 1998). These features in Fig. 21 indicate that in the case of Kwajalein, the three cloud categories suggested by Johnson et al. (1999) were affecting the distribution but not producing individual modal peaks.

4. Characteristics of the largest echoes: MCSs at Kwajalein

During the KWAJEX time period, La Niña conditions were prevalent, leading to a suppressed level of large-scale convective activity (Sobel et al. 2004; Y05). Only three MCSs passed through the radar domain during the KWAJEX time period. To analyze a larger sample of MCSs, the multiyear Kwajalein dataset was exploited to identify and characterize 21 MCSs occurring between the beginning of the KWAJEX time period (July 1999) through December 2000, as explained in section 2a.

a. Synoptic conditions

Reed and Recker (1971) noted the dominance of westward-propagating synoptic-scale disturbances in the equatorial western Pacific, and Straub and Kiladis

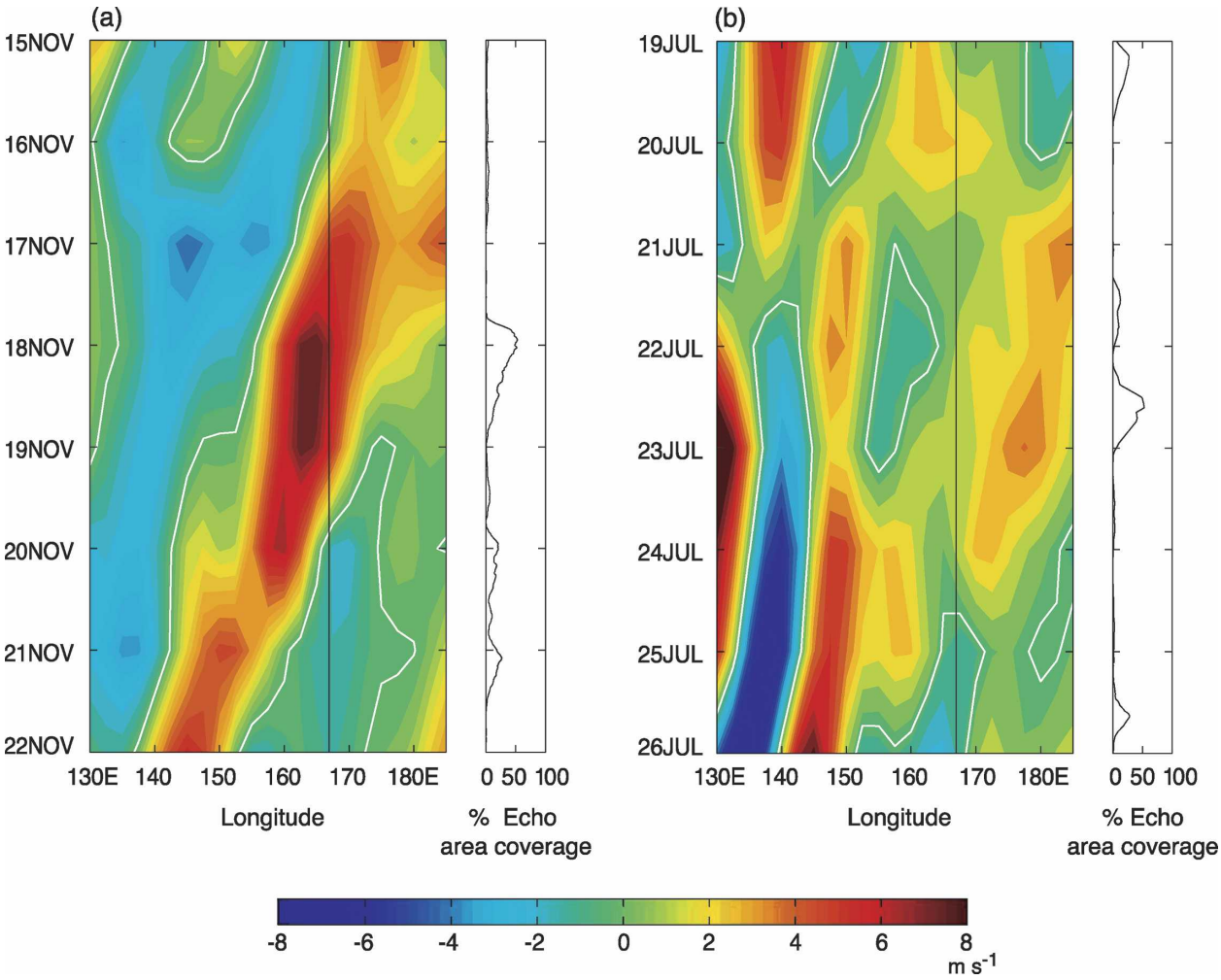

FIG. 22. (colored panels) The NCEP 850-hPa meridional wind at 10°N, as a function of time and longitude, and (noncolored panels) the corresponding time series of the fractional echo area coverage at Kwajalein during two times of MCSs at Kwajalein: (a) 15–22 Nov 1999 and (b) 19–26 Jul 2000. Black line indicates longitude of Kwajalein.

(2002) found that eastward-propagating Kelvin waves are also common in the region. Sobel et al. (2004) studied the synoptic-scale conditions associated with the three MCSs seen by the KR during KWAJEX. They found that westward-propagating mixed Rossby gravity waves and tropical depression–type waves, as well as eastward-propagating Kelvin waves, played a role in the development of the three MCSs.

Analysis of the synoptic conditions surrounding the 18 other MCSs provided evidence that the appearance of an MCS in the Kwajalein region systematically coincides with a westward-propagating disturbance. Figures 22a,b present time–longitude plots of the National Centers for Environmental Prediction (NCEP) 850-hPa meridional wind at 10°N across the west Pacific and the percentage of echo area coverage on the KR during two of the analyzed MCS. These two cases occurred outside the KWAJEX time period and were thus not included in the analysis of Sobel et al. (2004). Large peaks in aerial coverage indicate times when MCSs are present. In Fig. 22a, the presence of a large peak in echo area coverage (>50% on 18 November) occurs during a time of strong southerlies moving westward through the Kwajalein region (indicated by the black line). Similarly, Fig. 22b shows another >50% peak in echo area coverage coinciding with a westward-propagating southerly wind anomaly on 22 July. These examples are typical of the analyzed MCSs. They tended to form during times of anomalously strong southerlies propagating across the Pacific, and these MCSs tended to pass through the Kwajalein region around the time of the maximum southerly anomaly.

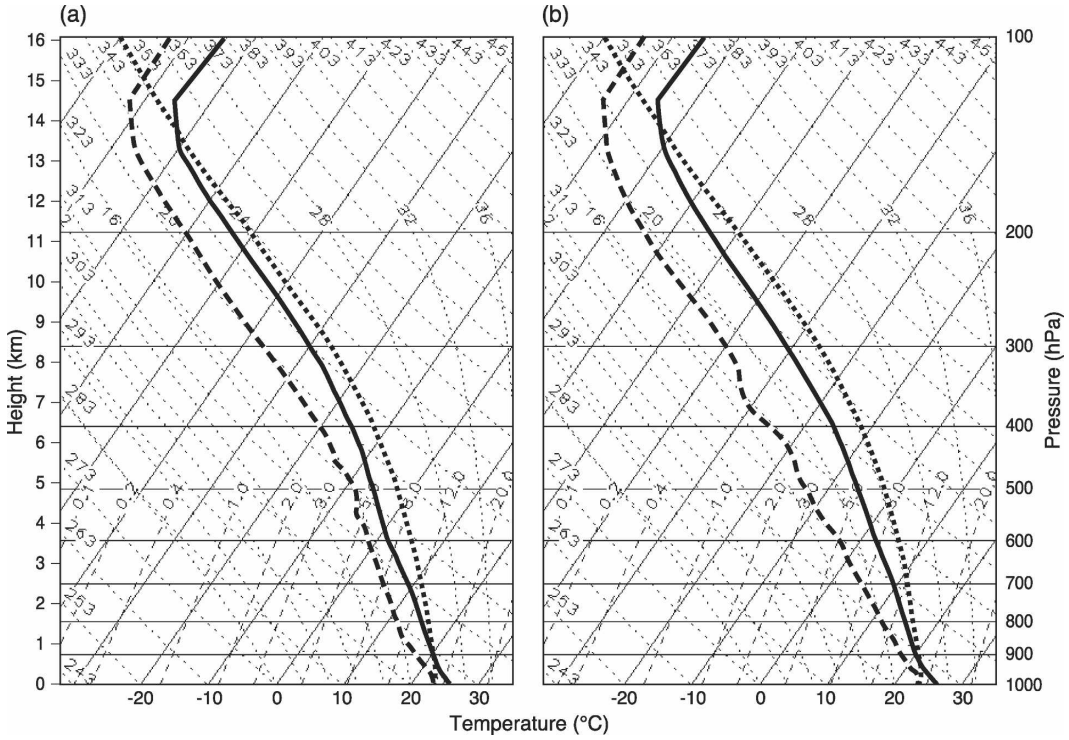

FIG. 23. Average thermodynamic soundings for times when (a) MCSs are present and (b) non-MCS convective echoes are present. Temperatures are indicated by the heavy solid line, dewpoint temperatures by the heavy dashed line, and temperatures of lifted surface parcels by the dotted line.

b. Horizontal motion

The MCSs moved with the large-scale flow in the Kwajalein region. All but 2 of the 21 analyzed MCSs at Kwajalein moved in a predominantly westward direction. The two other systems followed a northward track. In all cases, the systems moved according to the direction of the low-level wind (1000 to ~600 hPa). Although the systems as a whole moved with the low-level winds, certain features propagated in different directions and at different speeds within each system. Convective areas or bands tended to move in the direction that the system as a whole moved, but faster. Individual decaying cells moved back into the stratiform region. Often, the stratiform region moved much slower than the convective cells or even appeared to be stationary. Since the active stratiform cloud deck lies generally above the melting level, this behavior likely resulted from the change of the environmental wind above the 600-hPa level.

c. Thermodynamics

Average soundings for times when MCSs are present and times of ordinary convection at Kwajalein are plotted in Figs. 23a,b, respectively. When the MCS soundings are compared to the deep echo soundings from section 3b and Figs. 9 and 10, we see very little similarity. The deep echo sounding is more similar to the non-MCS sounding in the profiles of potential temperature, equivalent potential temperature, mixing ratio, and the values of CAPE. This indicates that the environment that creates MCSs is markedly different from the environment that creates isolated, deep convection.

In comparing the MCS and non-MCS soundings in Fig. 23, most apparent is the humidity difference between the two soundings. The dewpoint temperatures from the surface to approximately 800 hPa are almost identical for both soundings. However, the rest of the troposphere above 800 hPa is significantly moister in the MCS sounding. Relative humidities during times of MCSs are 10%–45% greater than times of normal convection at these levels. The moister midtroposphere and drier lower troposphere for the MCS cases is also evident in mixing ratio profiles (Fig. 24c). We also note the lower near-surface value of θ, indicative of downdrafts (below ~950 hPa in Fig. 24c). These structures suggest that the environments of the MCSs had been overturned by previous convection. However, other factors may also have been involved.

Also apparent in Fig. 23a (the MCS sounding) is the

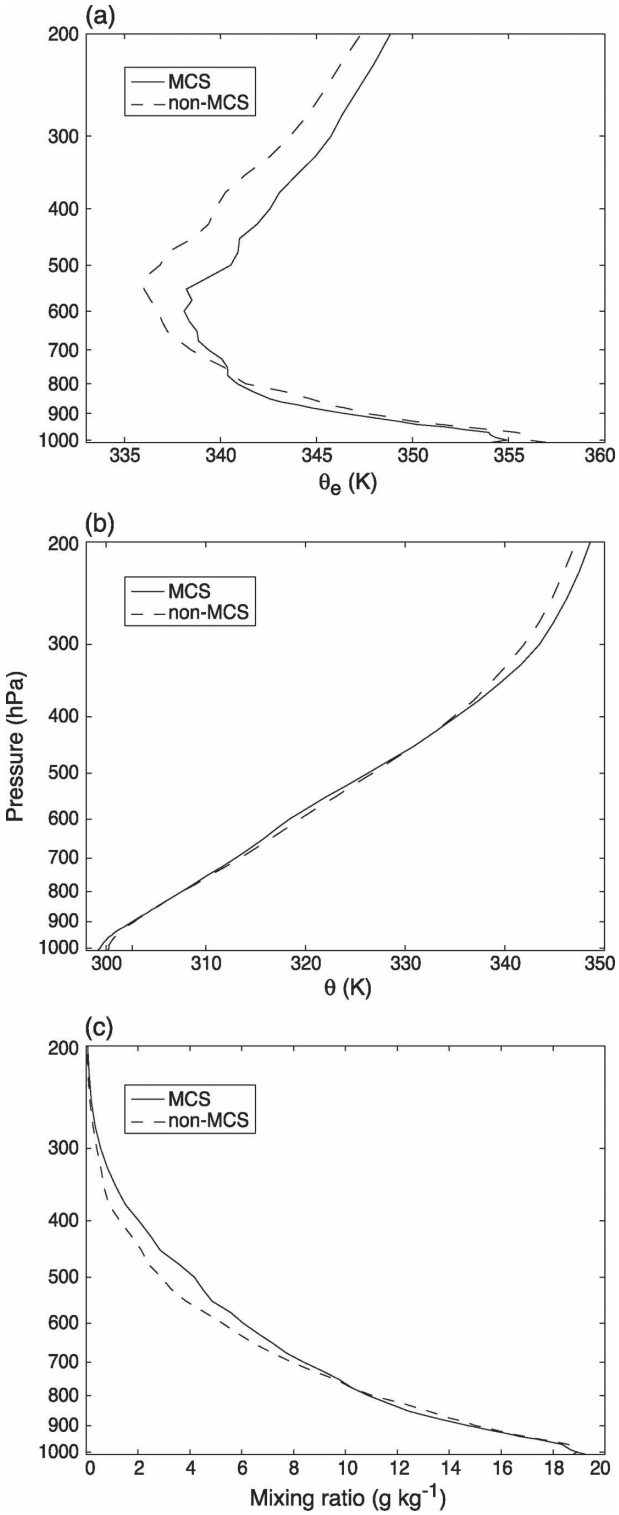

FIG. 24. Vertical profiles of (a) equivalent potential temperature, (b) potential temperature, and (c) mixing ratio for times when MCSs are present and non-MCS convective echoes are present as derived from the thermodynamic soundings in Fig. 23.

enhanced buoyancy (thin dashed line) of a rising boundary layer parcel passing through the 700–550-hPa layer. The enhanced buoyancy is indicated by the greater difference between the lifted parcel temperature and the environmental temperature in this layer compared to the non-MCS sounding. This difference is also evident in Fig. 24b, which indicates lower potential temperatures in the 700–500-hPa region of the MCS and suggests that the greater instability is at least in part thermally produced rather than owing simply to environmental humidity differences between MCS and non-MCS cases. The greater parcel buoyancy indicates greater parcel acceleration in the midlevels, which corresponded to a greater ability for the parcels to penetrate to higher levels in the MCS case. Although the environment during times of MCSs had likely already been previously mixed by recent convection, there remained the potential for more robust convection than during times of non-MCS convection via the thermal instability. Both the enhanced humidity and the greater buoyancy in the mid- and upper troposphere in the MCS environment could have been a result of deep synoptic-scale lifting, associated with the westward-propagating disturbances of the type illustrated in Fig. 22. In investigations of eastern Pacific tropical convection Serra and Houze (2002) and Petersen et al. (2003) have also found evidence that synoptic-scale wave modulation of the soundings is associated with deep convective behavior.

Another notable difference in the MCS and non-MCS cases is the occurrence of greater environmental conditional instability in the lower troposphere during times of MCS echoes, as evidenced by the increased vertical gradient of θ_e in the lower troposphere (~950–800 hPa), just above the thin surface layer of downdraft cooling and drying (located below ~950 hPa). More total CAPE was present during times of non-MCS convection (2248 J kg^{-1}) than during times of MCSs (1687 J kg^{-1}). However, the CAPE measures the integrated buoyancy over the full depth of the troposphere and may not accurately indicate the occurrence of convection when the instability is concentrated in the lower troposphere and the midlevels are moist and relatively free of inhibiting entrainment after moist parcels initiated in the lower troposphere move up into the midtroposphere.

d. Kinematics

The KR has Doppler capabilities and therefore the radial velocity of the echoes can be analyzed to infer the internal circulation of the MCSs. The internal kinematics of MCSs in other large-scale settings have been well documented by previous studies (e.g., Zipser 1969;

Moncrieff and Green 1972; Moncrieff and Miller 1976; Moncrieff 1978, 1981, 1985, 1992; Thorpe et al. 1982; Miller and Moncrieff 1983; Moncrieff and Klinker 1997; Houze et al. 1989, 1990; Kingsmill and Houze 1999; Fritsch and Forbes 2001; Houze et al. 2000; Mechem et al. 2002; Houze 2004). This previous literature shows that MCSs differ from singular convective elements in that the flow becomes organized into readily identifiable deep layers (referred to by Thorpe et al. 1982 and Moncrieff 1992 as the jump updraft, overturning updraft, and downdraft). Kingsmill and Houze (1999) noted that the subsiding midlevel stratiform inflow [Moncrieff's (1992) downdraft] started above the 0°C level and crossed the melting layer on its descent. As suggested by Houze (1982, 1989) and Houze et al. (2000), these mesoscale circulations are capable of strong heating and momentum feedbacks to the large-scale flow.

Figure 25 shows vertical cross sections of radar reflectivity and earth-relative radial velocity through a mature MCS seen by the KR. The system was moving from right to left in these figures. From the reflectivity image, it is clear that this was a leading convective region followed by a region of trailing stratiform rain. Superimposed on these images are hypothesized streamlines, consistent with the Moncrieff paradigm and with the observed radial velocity field in Fig. 25b. The indicated flow is similar to that of Fig. 25 of Kingsmill and Houze (1999), complete with an overturning convective updraft, rear updraft outflow, stratiform outflow, and a downward-sloping stratiform inflow that connects with a downdraft outflow. With the flow superimposed on the reflectivity field, it is clear that the updrafts are associated with the convective cell, and that the rear inflow and downdraft regions are associated with the stratiform precipitation, as described by Moncrieff (1992) and Kingsmill and Houze (1999). The midlevel stratiform inflow crosses the 0°C level, which is indicated by the radar bright band. From this example, as well as the other cases not shown, it is evident that the MCSs at Kwajalein conform to the standard models.

5. Conclusions

The ensemble characteristics of the oceanic radar echo population in the vicinity of Kwajalein exhibits lognormal or truncated lognormal frequency distributions of echo area, height, and duration, similar to the echo populations in other regions of the Tropics. The echo area distributions were nearly identical to those observed in GATE over the eastern tropical Atlantic (except for the largest areas). The echo heights were slightly greater at Kwajalein and were associated with two midtropospheric humidity minima. When these humidity minima were absent, the echoes extended higher. Echo durations were generally less at Kwajalein than in GATE. The echo lifetimes at Kwajalein were more highly affected by merging and splitting than in GATE.

Echo area was correlated with height, similar to GATE. However, unlike GATE, the KWAJEX echoes exhibited almost no correlation between echo area and duration, except for the very large MCS echoes, which were very long lived. This result is an outcome of the more frequent truncation of lifetimes by merging and splitting in the Kwajalein region.

The KWAJEX echoes moved faster than the GATE echoes, averaging $\sim 6\ \mathrm{m\ s^{-1}}$ when squall lines were omitted. There was a very weak correlation between echo area and speed, whereas the GATE echoes displayed no correlation. The Kwajalein echoes tracked most closely with the 700-hPa winds, whereas the GATE echoes generally tracked well with slightly lower winds (~850 hPa), consistent with the GATE echoes being somewhat shallower.

One of the most interesting results was the existence of a pronounced bimodal distribution of echo orientation angles at Kwajalein. These two orientation modes are at right angles to each other and, when compared to the low-level shear vector, these two modes were found to be shear parallel and shear normal, respectively. The result of shear-parallel- and shear-normal-oriented echoes has been noted previously (Barnes and Sieckman 1984; LeMone et al. 1998; Johnson et al. 2005) as having different propagation speeds, but the two modes at Kwajalein did not display this characteristic; they moved at similar speeds, likely due to the masking of any dynamic differences of the two modes by the strong trade winds. The shear-parallel and shear-normal modes often coexisted, indicating a potential difficulty in predicting or parameterizing line orientations in terms of large-scale variables.

The larger echoes at Kwajalein contained more numerous convective cores, but also had larger stratiform components. The height distribution of the convective cores was not inconsistent with the existence of three modes of convection (Johnson et al. 1999), but the distribution did not exhibit separate peaks at the expected three modes.

As found by Sobel et al. (2004), MCSs at Kwajalein tended to occur in connection with synoptic-scale disturbances. We confirmed this result for a broader sample of data than the KWAJEX period examined by Sobel et al. (2004). The Kwajalein MCSs documented in our study generally moved with the low–midtropo-

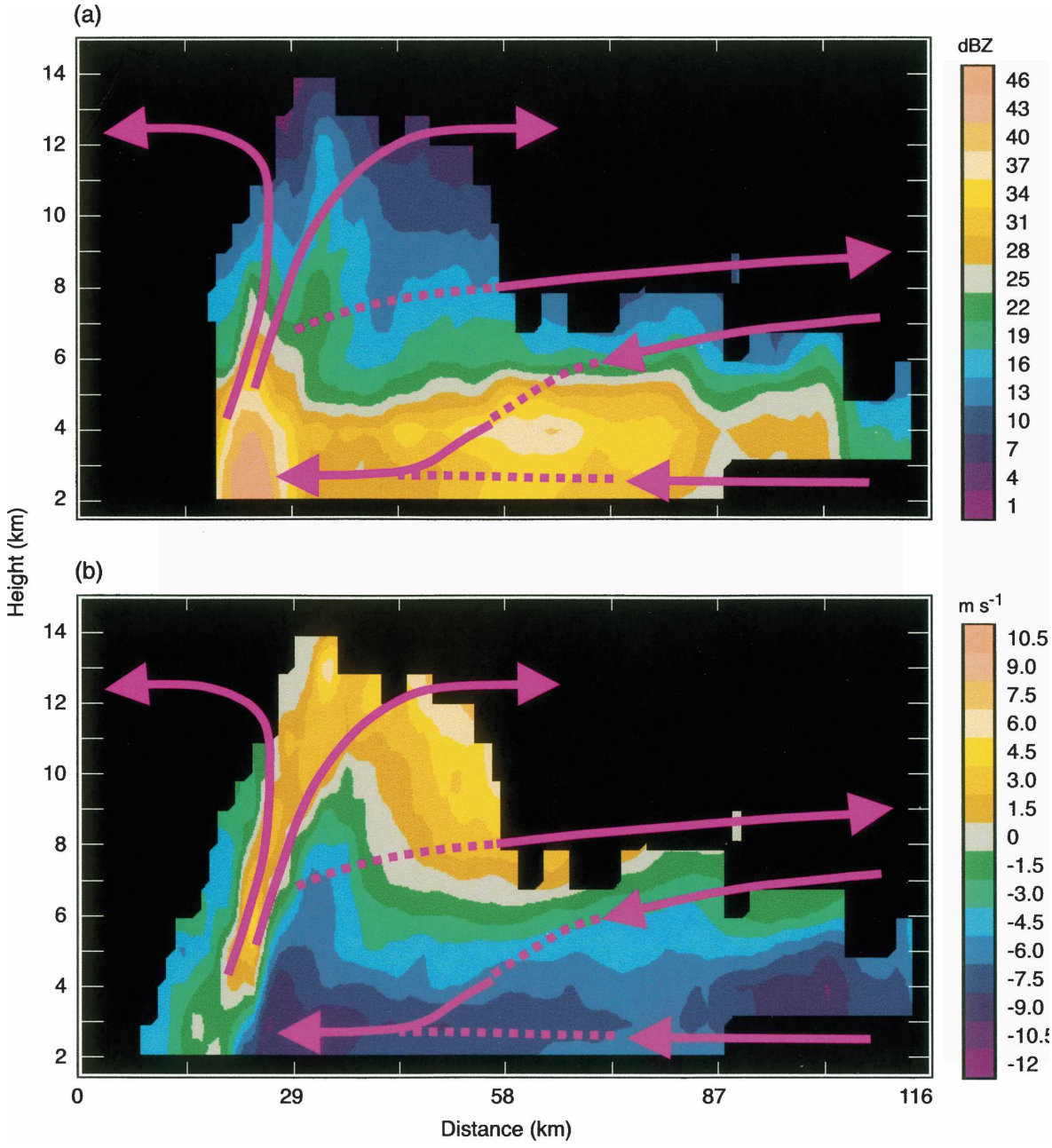

FIG. 25. Radar vertical cross sections of (a) reflectivity and (b) radial velocity through a mature MCS at 2236 UTC 11 Aug 1999. The radar is located to the left of each figure. In (b), positive values denote flow away from the radar (i.e., from left to right). Pink lines denote approximated flow fields as determined from the radial velocity image. The flow fields are adapted from idealized flow fields through MCSs as determined by Kingsmill and Houze (1999, their Fig. 25).

spheric flow (1000–600-hPa winds), which had a dominantly easterly component. Occasionally an MCS would move southerly. Soundings indicated that there was more tropospheric moisture and lower-tropospheric buoyancy during times of MCSs, although there was less CAPE. Analysis of the Doppler radial velocity data showed that the MCSs at Kwajalein exhibited characteristics seen in other studies of tropical MCSs (Moncrieff 1992; Kingsmill and Houze 1999), including the existence of an overturning updraft, jump updraft, and stratiform inflow that crosses the melting layer.

Overall, the gross convective population characteristics in the vicinity of Kwajalein resemble those seen in previous studies of tropical convective populations. Evidently, the convective ensembles exhibit similar dis-

tributions from one tropical oceanic region to another, but the parameters of the distributions vary. Comparison of the Kwajalein and GATE convective populations suggest that factors such as the sea surface temperature, winds, humidity, and continental influences lead to somewhat different distribution parameters in the two regions. For example, we might speculate that the higher sea surface temperature at Kwajalein leads to a more crowded convective population with concomitant greater frequency of echo lifetimes and a lower correlation of echo area and height. Also, the proximity to the Saharan air layer in the case of GATE probably led to a drier midlevel environment, more destructive entrainment, and a lower mean echo height. These characteristics suggest that there is an observational basis for parameterizing the population properties of oceanic tropical convection in terms of large-scale environmental conditions. However, the coexistence of multiple modes of convective organization (e.g., the shear-parallel and shear-normal lines of convection) and the wide spread of values even among correlated variables suggest that accurate parameterization will be subtle and complex.

Acknowledgments. Professors Sandra Yuter and Bradley Smull provided helpful comments. Candace Gudmundson edited the manuscript and Beth Tully refined the figures. Valuable data processing assistance was provided by Stacy Brodzik and Sean Casey. Two anonymous reviewers provided insightful comments. This research was supported by NASA Grants NAG5-9668 and NAG5-13654 and by an American Meteorological Society Fellowship, sponsored by the Department of Energy Atmospheric Radiation Measurement Program.

REFERENCES

Barnes, G. M., and K. Sieckman, 1984: The environment of fast- and slow-moving tropical mesoscale convective cloud lines. *Mon. Wea. Rev.,* **112,** 1782–1794.

Carlson, T. N., and J. M. Prospero, 1972: The large-scale movement of Saharan air outbreaks over the northern equatorial Atlantic. *J. Appl. Meteor.,* **11,** 283–297.

Cheng, C.-P., and R. A. Houze Jr., 1979: The distribution of convective and mesoscale precipitation in GATE radar echo patterns. *Mon. Wea. Rev.,* **107,** 1370–1381.

Churchill, D. D., and R. A. Houze Jr., 1984: Development and structure of winter monsoon cloud clusters on 10 December 1978. *J. Atmos. Sci.,* **41,** 933–960.

Corbet, J., C. Mueller, C. Burghart, K. Gould, and G. Granger, 1994: Zeb: Software for integration, display, and management of diverse datasets. *Bull. Amer. Meteor. Soc.,* **75,** 783–792.

Dunion, J. P., and C. S. Velden, 2004: The impact of the Saharan air layer on Atlantic tropical cyclone activity. *Bull. Amer. Meteor. Soc.,* **85,** 353–365.

Fritsch, J. M., and G. S. Forbes, 2001: Mesoscale convective systems. *Severe Convective Storms, Meteor. Monogr*., No. 50, 323–357.

Houze, R. A., Jr., 1982: Cloud clusters and large-scale vertical motions in the tropics. *J. Meteor. Soc. Japan,* **60,** 396–410.

——, 1989: Observed structure of mesoscale convective systems and implications for large-scale heating. *Quart. J. Roy. Meteor. Soc.,* **115,** 425–461.

——, 1993: *Cloud Dynamics*. Academic Press, 573 pp.

——, 1997: Stratiform precipitation in regions of convection: A meteorological paradox? *Bull. Amer. Meteor. Soc.,* **78,** 2179–2196.

——, 2004: Mesoscale convective systems. *Rev. Geophys.,* **42,** RG4003, doi:10.1029/2004RG000150.

——, and C.-P. Cheng, 1977: Radar characteristics of tropical convection observed during GATE: Mean properties and trends over the summer season. *Mon. Wea. Rev.,* **105,** 964–980.

——, ——, C. A. Leary, and J. F. Gamache, 1980: Diagnosis of cloud mass and heat fluxes from radar and synoptic data. *J. Atmos. Sci.,* **37,** 754–773.

——, S. A. Rutledge, M. I. Biggerstaff, and B. F. Smull, 1989: Interpretation of Doppler weather radar displays in midlatitude mesoscale convective systems. *Bull. Amer. Meteor. Soc.,* **70,** 608–619.

——, B. F. Smull, and P. Dodge, 1990: Mesoscale organization of springtime rainstorms in Oklahoma. *Mon. Wea. Rev.,* **118,** 613–654.

——, S. S. Chen, D. E. Kingsmill, Y. Serra, and S. E. Yuter, 2000: Convection over the Pacific warm pool in relation to the atmospheric Kelvin-Rossby wave. *J. Atmos. Sci.,* **57,** 3058–3089.

——, S. Brodzik, C. Schumacher, S. E. Yuter, and C. R. Williams, 2004: Uncertainties in oceanic radar rain maps at Kwajalein and implications for satellite validation. *J. Appl. Meteor.,* **43,** 1114–1132.

Hudlow, M. D., 1979: Mean rainfall patterns for the three phases of GATE. *J. Appl. Meteor.,* **18,** 1656–1669.

——, R. Arkell, V. Patterson, P. Pytlowany, F. Richards, and S. Geotis, 1979: Calibration and intercomparison of the GATE C-Band radars. NOAA Tech. Rep., EDIS, 31, 98 pp.

Iwanchuk, R. M., 1973: Characteristics and distribution of precipitation areas over the tropical Atlantic. M.S. thesis, Dept. of Meteorology, MIT, Cambridge, MA, 106 pp.

Johnson, R. H., T. M. Rickenbach, S. A. Rutledge, P. E. Ciesilski, and W. H. Schubert, 1999: Trimodal characteristics of tropical convection. *J. Climate,* **12,** 2397–2418.

——, S. A. Aves, P. E. Ciesielski, and T. D. Keenan, 2005: Organization of oceanic convection during the onset of the 1998 East Asian summer monsoon. *Mon. Wea. Rev.,* **133,** 131–148.

Kingsmill, D. E., and R. A. Houze Jr., 1999: Kinematic characteristics of air flowing into and out of precipitating convection over the west Pacific warm pool. *Quart. J. Roy. Meteor. Soc.,* **125,** 1165–1207.

LeMone, M. A., E. J. Zipser, and S. B. Trier, 1998: The role of environmental shear and thermodynamic conditions in determining the structure and evolution of mesoscale convective systems during TOGA COARE. *J. Atmos. Sci.,* **55,** 3493–3518.

López, R. E., 1976: Radar characteristics of the cloud populations of tropical disturbances in the northwest Atlantic. *Mon. Wea. Rev.,* **104,** 268–283.

——, 1977: The lognormal distribution and cumulus cloud populations. *Mon. Wea. Rev.,* **105,** 865–872.

Mechem, D. B., R. A. Houze Jr., and S. S. Chen, 2002: Layer inflow into precipitating convection over the western tropical Pacific. *Quart. J. Roy. Meteor. Soc.,* **128,** 1997–2030.

Miller, M. J., and M. W. Moncrieff, 1983: Dynamics and simulation of organized deep convection. *Mesoscale Meteorology—Theory, Observations and Models,* D. K. Lilly and T. Gal-Chen, Eds., NATO Advanced Study Institute Series C: Mathematical and Physical Sciences, Vol. 114, D. Reidel, 451–496.

Moncrieff, M. W., 1978: The dynamical structure of two-dimensional steady convection in constant vertical shear. *Quart. J. Roy. Meteor. Soc.,* **104,** 543–568.

——, 1981: A theory of organized steady convection and its transport properties. *Quart. J. Roy. Meteor. Soc.,* **107,** 29–50.

——, 1985: Steady convection in pressure coordinates. *Quart. J. Roy. Meteor. Soc.,* **111,** 857–866.

——, 1992: Organized convective systems: Archetypal dynamical models, mass and momentum flux theory, and parametrization. *Quart. J. Roy. Meteor. Soc.,* **118,** 819–850.

——, and J. S. A. Green, 1972: The propagation and transfer properties of steady convective overturning in shear. *Quart. J. Roy. Meteor. Soc.,* **98,** 336–352.

——, and M. J. Miller, 1976: The dynamics and simulation of tropical squall lines. *Quart. J. Roy. Meteor. Soc.,* **102,** 373–394.

——, and E. Klinker, 1997: Organized convective systems in the tropical western Pacific as a process in general circulation models: A TOGA COARE case study. *Quart. J. Roy. Meteor. Soc.,* **123,** 805–827.

Petersen, W. A., R. Cifelli, D. J. Boccippio, S. A. Rutledge, and C. Fairall, 2003: Convection and easterly wave structures observed in the eastern Pacific warm pool during EPIC-2001. *J. Atmos. Sci.,* **60,** 1754–1773.

Rangno, A. L., and P. V. Hobbs, 2005: Microstructures and precipitation development in cumulus and small cumulonimbus clouds over the warm pool of the tropical Pacific Ocean. *Quart. J. Roy. Meteor. Soc.,* **131,** 639–673.

Reed, R. J., and E. E. Recker, 1971: Structure and properties of synoptic-scale wave disturbances in the equatorial western Pacific. *J. Atmos. Sci.,* **28,** 1117–1133.

Rickenbach, T. M., and S. A. Rutledge, 1998: Convection in TOGA COARE: Horizontal scale, morphology, and rainfall production. *J. Atmos. Sci.,* **55,** 2715–2729.

Rossow, W. B., A. W. Walker, D. E. Beuschel, and M. D. Roiter, 1996: International Satellite Cloud Climatology Project (ISCCP) documentation of new cloud datasets. WMO/TD-737, World Climate Research Programme, Geneva, Switzerland, 115 pp.

Saunders, P. M., 1965: Some characteristics of tropical marine showers. *J. Atmos. Sci.,* **22,** 167–175.

Schumacher, C., and R. A. Houze Jr., 2000: Comparison of radar data from the TRMM satellite and Kwajalein oceanic validation site. *J. Appl. Meteor.,* **39,** 2151–2164.

——, and ——, 2003a: Stratiform rain in the Tropics as seen by the TRMM precipitation radar. *J. Climate,* **16,** 1739–1756.

——, and ——, 2003b: The TRMM precipitation radar's view of shallow, isolated rain. *J. Appl. Meteor.,* **42,** 1519–1524.

Serra, Y., and R. A. Houze Jr., 2002: Observations of variability on synoptic timescales in the east Pacific ITCZ. *J. Atmos. Sci.,* **59,** 1723–1743.

Sobel, A. H., S. E. Yuter, C. S. Bretherton, and G. N. Kiladis, 2004: Large-scale meteorology and deep convection during TRMM KWAJEX. *Mon. Wea. Rev.,* **132,** 422–444.

Steiner, M., R. A. Houze Jr., and S. E. Yuter, 1995: Climatological characterization of three-dimensional storm structure from operational radar and rain gauge data. *J. Appl. Meteor.,* **34,** 1978–2007.

Straub, K. H., and G. N. Kiladis, 2002: Observations of a convectively coupled Kelvin wave in the eastern Pacific ITCZ. *J. Atmos. Sci.,* **59,** 30–53.

Thorpe, A. J., M. J. Miller, and M. W. Moncrieff, 1982: Two-dimensional convection in non-constant shear: A model of mid-latitude squall lines. *Quart. J. Roy. Meteor. Soc.,* **108,** 739–762.

Williams, M., and R. A. Houze Jr., 1987: Satellite-observed characteristics of winter monsoon cloud clusters. *Mon. Wea. Rev.,* **115,** 505–519.

Yuter, S. E., and R. A. Houze Jr., 1997: Measurements of raindrop size distributions over the Pacific warm pool and implications for *Z–R* relations. *J. Appl. Meteor.,* **36,** 847–867.

——, ——, E. A. Smith, T. T. Wilheit, and E. Zipser, 2005: Physical characterization of tropical oceanic convection observed in KWAJEX. *J. Appl. Meteor.,* **44,** 385–415.

Zipser, E. J., 1969: The role of organized unsaturated convective downdraughts in the structure and rapid decay of an equatorial disturbance. *J. Appl. Meteor.,* **8,** 779–814.